

# Light front QED<sub>1+1</sub> at finite temperature

S. Strauss\* and M. Beyer†  
*Institute of Physics, University of Rostock,  
18051 Rostock, Germany*

(Dated: November 20, 2018)

We investigate thermodynamic properties of quantum electrodynamics in 1 + 1 dimensions (QED<sub>1+1</sub>) utilizing light front dynamics. Therefore we derive the partition function of the canonical ensemble in discrete light cone quantization, and calculate the thermodynamical potential. This central quantity is evaluated for different system sizes and coupling strengths. We investigate the continuum limit and the thermodynamical limit and present basic thermodynamical quantities such as pressure, energy, and entropy, as a function of temperature for the interacting system. The results are compared to the ideal bosonic and fermionic cases.

PACS numbers: 05.30.-d,11.10.Wx, 11.10.Kk,11.15.Tk,12.20.-m,

Recently, Light Front Quantization (LFQ) originally introduced by Dirac in 1949 [1] has been successfully extended to relativistic systems of finite temperatures  $T$ , and also chemical potentials  $\mu$  [2, 3, 4, 5, 6, 7, 8]. The interest in utilizing LFQ in the area of quantum statistics and thermo-field theory is motivated through the need to investigate strongly coupled relativistic systems. A pertinent example of such a system is given by the quark gluon plasma (QGP), that is a new state of matter recently discovered at the relativistic heavy ion collider (RHIC) [9].

Practical use of LFQ as a nonperturbative method to treat strongly interacting systems has been realized through Discrete Light Cone Quantization (DLCQ) introduced in [10]. Subsequently DLCQ has been used to treat two-dimensional gauge theories like Quantum Electrodynamics QED<sub>1+1</sub> [11, 12] and Quantum Chromodynamics QCD<sub>1+1</sub> [13]. Following these promising applications of DLCQ many other models of various dimensions have been investigated. Further progress in the Light front Schwinger model has been obtained utilizing the Tamm-Dancoff approximation [14, 15]. Besides the LFQ approach finite lattice size computations have been performed, see e.g. Refs. [16, 17] and refs. therein. Alternatively, an instant form Hamiltonian lattice approach in a fast moving frame was shown to give reasonable results [18]. The interest in QED<sub>1+1</sub> is motivated by the appearance of phenomena like chiral symmetry breaking, charge confinement, and topological properties associated to  $\theta$  vacua similar to full QCD. In addition, it is a widely studied theory to investigate new solution methods like the one presented here.

In the initial work of Ref. [2] that focused on finite temperatures, DLCQ was merely introduced to compute the mass spectrum of QED<sub>1+1</sub>. Subsequently, the mass spectrum has then been used in an instant form framework to determine thermodynamic quantities like the partition

function, internal energy, specific heat, etc. In this framework the authors obtained remarkable results including a second order phase transition at around  $T \simeq 1 g/\sqrt{\pi}$  (where the strength  $g$  will be specified below). Extrapolation to the continuum limit leads to a lower bound for the critical exponent  $\alpha > 0.7$  and critical temperatures  $T_c = 0.5 \dots 1.0 g/\sqrt{\pi}$  (depending on the interaction) even in the strong coupling regime, where the Schwinger model is exactly solvable by bosonization. This is astonishing, since in a correct treatment of the two limits, (i) weak coupling  $m/g \rightarrow \infty$  and (ii) strong coupling  $m/g \rightarrow 0$  (where  $m$  is the mass unit, see below), a free fermion respectively a free boson equation of state (EOS) should be realized.

Within the same framework of [2] Hiller et al. investigated a super-symmetric model in two dimensions [19, 20]. They computed thermodynamic observables of the bosonic and fermionic sectors of the theory. It turns out that irrespective of the specific findings of Ref. [2] the models under concern [19, 20] due to the large  $N_c$  limit lead to a free theory of mesonic states. As a consequence the EOS is trivially that of an ideal system of bosons.

In order to study the non-ideal case we investigate the massive chiral Schwinger model for interaction terms of finite values of  $m/g$ . We first solve the DLCQ Hamiltonian up to some harmonic resolution and then evaluate the proper partition function for finite temperature without introducing any quasi particle concept. The continuum and the thermodynamic limits are carefully performed.

We introduce the massive chiral Schwinger model in DLCQ following Refs. [11, 12]. Within the DLCQ approach the light-like physical extension  $x^-$  is restricted to  $-L/2 \leq x^- \leq L/2$ . Therefore by demanding (anti)-periodic boundary conditions of the fields the conjugate momentum variable  $p^+$  becomes discrete  $p_n^+ = \frac{2\pi}{L}n$ ,  $n \in \mathbb{N}$ . For periodic boundary conditions the  $n = 0$  mode (fermionic zero mode) exists while for anti-periodic boundary condition  $n > 0$  holds. In the following we choose light cone gauge  $A^+ = 0$  and neglect the fermionic and gauge zero modes to not obscure the thermodynamic

\*Electronic address: stefan.strauss@uni-rostock.de

†Electronic address: michael.beyer@uni-rostock.de

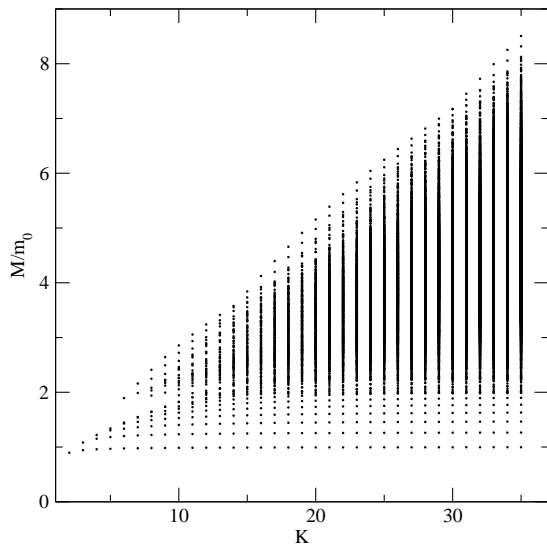


FIG. 1: Invariant mass spectrum of QED<sub>1+1</sub> for given harmonic resolutions  $K$  and  $m/g = 1$ .  $m_0$  denotes the lowest eigenvalue for  $K \rightarrow \infty$  and is used for normalization.

issues addressed here.

The light cone momentum operators can then be written as

$$P^+ = \frac{2\pi}{L}K, \quad P^- = \frac{L}{2\pi}H \quad (1)$$

with the harmonic resolution  $K$  being dimensionless and the LF Hamiltonian  $H$  of dimension mass squared. Expressed in Fock space creation/annihilation operators for particles ( $b_n^\dagger$ ) and antiparticles ( $d_n^\dagger$ ) the harmonic resolution and the free (dimensionless) Hamiltonian  $H_0$  are

$$K = \sum_{n=1}^{\Lambda} n (b_n^\dagger b_n + d_n^\dagger d_n), \quad (2)$$

$$H_0 = \sum_{n=1}^{\Lambda} \frac{1}{n} (b_n^\dagger b_n + d_n^\dagger d_n) \quad (3)$$

with a high momentum cutoff  $\Lambda$ . The full Hamiltonian is given by [11]

$$H = m^2 H_0 + \frac{g^2}{\pi} V = g^2 \left( \frac{m^2}{g^2} H_0 + \frac{1}{\pi} V \right), \quad (4)$$

where  $m$  is the bare mass and  $g$  the interaction strength. We have introduced the ratio  $m/g$  that for  $m/g \rightarrow 0$  gives the strong and  $m/g \rightarrow \infty$  the weak coupling limit. The Fock space representation of the potential  $V$  is a rather lengthy expression that has been given in Ref. [11] Sec. 2, and will not be repeated here for the sake of brevity.

We first determine the invariant mass spectrum  $M^2 = P^+ P^- = KH(K)$ . To do so, we construct the Fock space for a given resolution  $K$  and collect all possible

integer partitions  $\{K\}$ , where integers represent a single-particle momentum state of an electron or positron for a given momentum while the Pauli principle is observed. The Hamiltonian is block-diagonal in  $K$  and the resulting Fock space spanned by  $\{K\}$  is finite. We then calculate the DLCQ QED<sub>1+1</sub> Hamiltonian matrix  $H(K)$ , which can be diagonalized for values of  $K \lesssim 35$  without much effort on today standard PCs. The mass spectrum  $M = \sqrt{KH(K)}$  is shown in Figure 1 as a function of  $K$ .

At larger  $K > 35$  the dimension of the mass matrix soon becomes rather large. We therefore restrict ourselves to the lower part of the mass spectrum. To this end we introduce standard Krylov space methods to determine the lowest eigenvalues as used e.g. in Fig. 2.

Since  $M^2 = KH(K)$  does not explicitly depend on  $L$ , the continuum limit is achieved by  $K \rightarrow \infty$  which in turn implies for any given but (due to covariance) arbitrary  $P^+ > 0$  that  $L \rightarrow \infty$  (continuum). Assuming some low order fits explained below the continuum mass spectrum including an educated estimate of the error related to variation of the fit function or/and parameters is read off at  $1/K \rightarrow 0$ . This is demonstrated in Figure 2 for the binding energy  $E = M - 2m$  of the six lowest mass eigenvalues  $M$  for the case  $m/g = 1$ . In Table I we compare our results with earlier calculations [11, 14, 16, 17, 18] that have been given for the lowest two mass eigenvalues, the ground (vector) state and the first excited (scalar)

TABLE I: The different estimates for the bound state energies  $E_1/g$ ,  $E_2/g$  of the lowest two mass eigenstates at various  $m/g$ . For comparison the results of [14] and [11] using LCQ, finite-lattice results of [17] (first state), [16] (second state), and data obtained by the fast-moving frame lattice Hamiltonian method [18] are shown. Error given due to variation of extrapolating functions (The case  $g/m = 2^0$  is also shown in Fig. 2).

$m/g$	this work	[14]	[11]	[16], [17]	[18]
ground state / vector state					
$2^5$	0.191(3)	0.201	0.201	0.194(5)	0.191
$2^4$	0.2366(8)	0.224	0.228	0.238(5)	0.235
$2^3$	0.2856(4)	0.288	0.280	0.287(8)	0.285
$2^2$	0.33933(5)	0.337	0.338	0.340(1)	0.339
$2^1$	0.39355(4)	0.393	0.393	0.398(1)	0.394
$2^0$	0.4442(7)	0.444	0.444	0.4444(1)	0.445
$2^{-1}$	0.4873(1)	0.488	0.488	0.48747(2)	0.489
$2^{-2}$	0.519(1)	0.520	0.534	0.51918(5)	0.511
$2^{-3}$	0.538	0.540	0.603	0.53950(7)	0.528
first excited state / scalar state					
$2^5$	0.46(7)	0.458	0.458	0.45(1)	0.447
$2^4$	0.5623(3)	0.564	0.548	0.56(1)	0.559
$2^3$	0.696(4)	0.697	0.689	0.68(1)	0.690
$2^2$	0.839(2)	0.838	0.839	0.85(2)	0.837
$2^1$	0.9892(1)	0.989	0.985	1.00(2)	0.991
$2^0$	1.117(1)	1.119	1.126	1.12(3)	1.128
$2^{-1}$	1.2002(2)	1.201	1.228	1.20(3)	1.227
$2^{-2}$	1.21(3)	1.230	1.312	1.24(3)	1.279
$2^{-3}$	1.27(1)	1.219	1.407	1.22(2)	1.314

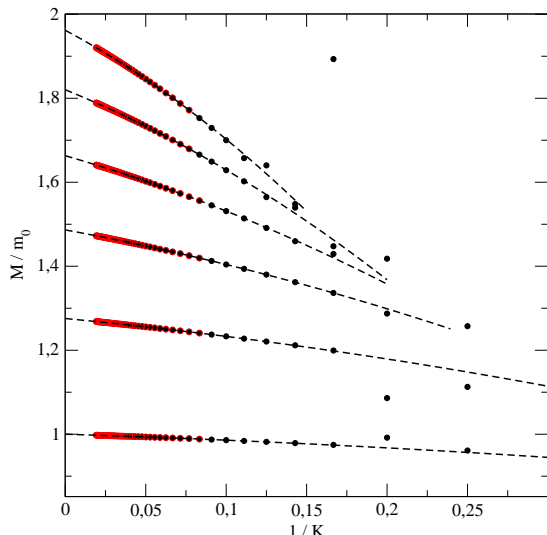


FIG. 2: The six lowest mass eigen values of  $\text{QED}_{1+1}$  as a function of  $1/K$  for  $m/g = 1$ . The dashed line is a quadratic fit to the data (values used in the fit are colored in red) and to extract the continuum limit.

state, for different interaction strengths  $m/g$ .

We use different extrapolation functions to extract the low lying masses depending on the coupling regime  $m/g$  to arrive at our results of Table I: At low coupling (that is  $m/g \geq 2^5$ ) the masses vary strongly and follow a linear curve in  $1/K$ , which is used in the fit, only for rather large resolutions  $K \geq 40$ . In the intermediate coupling regime  $2^{-1} \geq m/g \geq 2^4$  the light cone approach produces the most accurate results even for moderate  $K$ . However, a linear continuum extrapolation systematically gives too high estimates. Thus omitting the linear fit we do the analysis using second order polynomials. At small  $m/g$  ratios the scaling behavior is considerably different from the previous ones. Even at large resolution  $K$  the computed masses are still quite far away from the very precise continuum values found in [16, 17]. Changing the fit function to a polynomial in  $1/\sqrt{K}$  we obtain reasonable results at  $m/g = 2^{-2}$  but unstable ones at  $m/g = 2^{-3}$ . Therefore we do not indicate errors for the smallest  $m/g$  values but simply present our best fit estimates. All other errors have been determined through successive fits with next and next-to-next order power function applied to the same sample of data points. It is a well-known fact that ordinary LFQ does not capture all physics in the massless limit, e.g. ignores left moving fermions, that indicates why this approach has difficulties reaching the continuum. This can be cured by introducing a second light front [21] or near light cone coordinates [22]. Furthermore a proper inclusion of the gauge field zero mode following [23] should improve the convergence at small fermion mass. Interestingly, the bosonization of the massive chiral LC Schwinger model as suggested in Ref. [11] leads to different induced inertias, but otherwise leaves

the interaction  $V$  in (4) unchanged. The bosonized model gives exact results in the massless limit, however, even for strong coupling, similar uncertainties are present in the fermionic approach.

After solving the isolated DLCQ case to the present state of the art precision, we now turn to a canonical ensemble subject to the DLCQ Hamiltonian of  $\text{QED}_{1+1}$  given above. To calculate thermodynamic properties we evaluate the respective partition function that is the central quantity. Following the standard quantum statistical approach the partition function is evaluated by performing a trace over the statistical operator in the discretized Fock space. In LFQ the respective trace is given by

$$\begin{aligned} \mathcal{Z} &= \text{Tr} \exp\left\{-\frac{\beta}{2}(P^+ + P^-)\right\} \\ &= \sum_K \exp\left\{-\frac{\beta}{2} \frac{2\pi}{L} K\right\} \zeta_K, \quad \text{where} \quad (5) \\ \zeta_K &= \sum_{\{K\}} \exp\left\{-\frac{\beta}{2} \frac{L}{2\pi} \frac{M^2(\{K\})}{K}\right\}. \end{aligned}$$

The last two lines refer to the DLCQ expression, wherein the first part is the sum over the complete Fock space, and  $\zeta_K$  contains all Fock state partitions belonging to the given resolution  $K$ . The inverse temperature  $\beta = 1/(k_B T)$  ( $k_B$  Boltzmann constant) is the Lorentz invariant rest-frame temperature. In order to keep the standard definition of the temperature the (however kinematic)  $P^+$  component in the proper definition of the statistical operator on the light front appears in addition of the light front Hamiltonian  $P^-$ . Note that only for the interaction free case  $(P^+ + P^-)/2 = P^0$  can be replaced by  $P^0 = \sqrt{\vec{P}^2 + M^2}$ , where the Lorentz invariant mass eigenvalues  $M$  may be evaluated in any of the relativistic forms, e.g. light front form, as has been utilized in Refs. [2, 19, 20]. The case considered here, however, includes interactions and hence the evaluation of the trace becomes more cumbersome.

To give an instructive example, which is also used to estimate the theoretical error of the calculation, we evaluate the thermodynamic potential density  $\omega_f = \Omega_f/L$  for the canonical ensemble of the ideal fermi gas. The thermodynamical potential for two particle species is given as

$$\omega_f = -2T \int_0^\infty \frac{dp^+}{2\pi} \ln \left( 1 + \exp \left\{ -\beta \left( \frac{p^+}{2} + \frac{m^2}{2p^+} \right) \right\} \right), \quad (6)$$

where we set the mass to  $m = 0.5\text{MeV}$ . To compare (6) to the standard instant form expression, the r.h.s. can be directly transformed by a simple variable substitution. In the thermodynamic limit, the instant and light front form give equal results for the ideal case.

Evaluating the free thermodynamic potential density (6) for a given temperature will be referred to as the analytical result. To demonstrate our method this will be

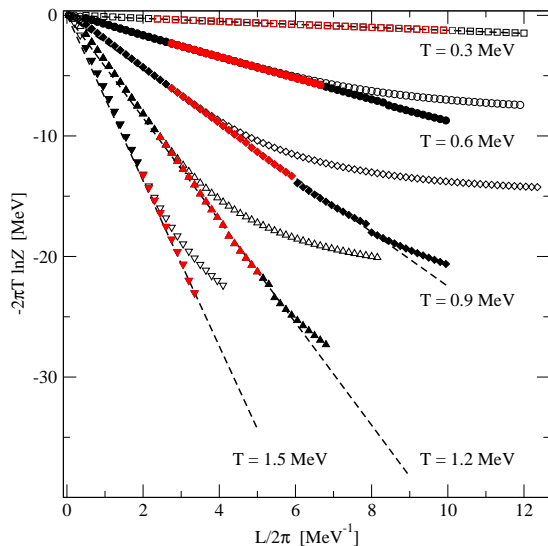


FIG. 3: The thermodynamical potential  $\Omega_f = -2\pi T \ln \mathcal{Z}$  as a function of  $L$ . Open symbols depict the potential at maximal resolution  $K = 110$  for the different temperatures. Closed symbols are given by the extrapolation as explained in the text. The slope of the linear part (values selected colored in red) is fitted to extract the invariant potential density.

compared in the following to the direct numerical evaluation of (5) for  $V = 0$  that depends on the length scale  $L$  and a maximum  $K$ . Since  $\ln \mathcal{Z}$  is an extensive property it scales with  $L$  as well as  $\omega = -T \ln \mathcal{Z}$ . For a given maximal harmonic resolution  $K$  the numerical results leads to  $\ln \mathcal{Z}$  as a function of the system size  $L$ . Hence  $\ln \mathcal{Z}$  can be read off the slope with respect to  $L$ . The situation for different temperatures is depicted in Figure 3. The analytic (exact) results are given as dashed lines and the numerical values as symbols, empty ones reflecting raw numerical data up to  $K = 110$ . The filled symbols are raw data corrected by a nonlinear fit as explained below. For large system sizes the harmonic resolution used in the evaluation is not sufficient, hence a deviation from the expected linear dependence of  $\ln \mathcal{Z}$  on  $L$  appears. For small  $L$  the system is too small to read off the thermodynamic limit, which also leads to a derivation (finite size effects). There is an optimal region of system sizes

TABLE II: Values of  $\ln \mathcal{Z}$  for the free fermi gas extracted from a linear fit to the numerical analysis along with the analytical results and the estimated uncertainties.

T [MeV]	$-2\pi T \ln \mathcal{Z}$ [MeV]		
	analytic	numeric	rel.error [%]
0.3	-0.124156	-0.124263	0.05
0.6	-0.862941	-0.863176	0.03
0.9	-2.24692	-2.24824	0.05
1.2	-4.24937	-4.24566	0.07
1.5	-6.85920	-6.76379	1.39

where  $\ln \mathcal{Z}$  depends almost linear on  $L$ , which is used to extract the slope by making a linear fit (indicated by red symbols in Fig. 3). In order to improve the numerical results we have used the following fitting algorithm for  $\mathcal{Z}$  of (5): Beyond the maximum of  $\mathcal{Z}$  we approximate  $\zeta_K$  by an exponential of  $\sum_{n=-2}^2 a_n K^n$ . The function depends on five parameters  $a_n$  that are determined by a  $\chi^2$ -fit to the largest 30 calculated  $K$ -values and then used for an extrapolation to larger  $K$ . The resulting values of  $\ln \mathcal{Z}$  for the four temperatures are given in Table II. The error indicated is the difference of the numerical from the analytic result. For small  $L$  the analytic value is approached from above and for large values it deviates again to larger values. As a consequence the slope (i.e.  $\ln \mathcal{Z}$ ) is usually slightly too steep. For the interacting case, where no exact analytic result is available, we utilize the same fitting procedure. Note however two differences to the pure fermionic case. First, particle number is not conserved because of an interacting field theory and, second, the charge  $Q$  of each state of the statistical ensemble is set to zero due to confinement. To be more explicit, the ideal fermionic (bosonic) gas as a limit of  $g/m \rightarrow 0$  ( $m/g \rightarrow 0$ ) has been evaluated for chemical potential  $\mu = 0$ . In the fermionic case this has to be done using the full numerical calculation obeying the condition  $Q = 0$ . However, the bosonic case can be worked out directly by evaluating the following integral

$$\omega_b = 2T \int_0^\infty \frac{dp^+}{2\pi} \ln \left( 1 - \exp \left\{ -\beta \left( \frac{p^+}{2} + \frac{1}{2p^+} \right) \right\} \right), \quad (7)$$

since Bose-Einstein condensation is absent in one dimension [24] (and would occur only at  $\mu = m$  for an ideal, relativistic bosonic gas in three dimensions).

In the reminder we give several thermodynamic quantities. Note that volume and temperature are now given in units of the ground state mass  $m_0$  that sets the scale of the interacting system. In Fig. 4 we show the pressure  $p = -\omega = T \ln \mathcal{Z}/L$  plotted as a function of temperature. Division is by  $T^2$  (rather than the usual  $T^4$ ) is due to the reduced dimension of the problem. The line shows the analytic result for the ideal bosonic case (limit  $m/g \rightarrow 0$ ) according to (7), the diamonds the ideal fermionic case (limit  $m/g \rightarrow \infty$ ). The other symbols represent two different interacting cases. The strong interacting one  $m/g = 2^{-3}$  (squares) is closer to the bosonic case, whereas the weak interacting one  $m/g = 1$  (circles) is closer to the ideal fermionic case. There is a smooth transition from the bosonic case to the fermionic case, depending on the interaction strength. In particular, we do not observe a critical behavior seen in [2] that might have been due to the rather low harmonic resolution used there. For  $T \rightarrow \infty$ , i.e. the classical ultrarelativistic case, masses can be neglected  $m \rightarrow 0$  and hence all curves approach  $p/T^2 = \pi/6$ . From Table I we assume a conservative mean error of 2.5% for the interacting case indicated in figures by error bars.

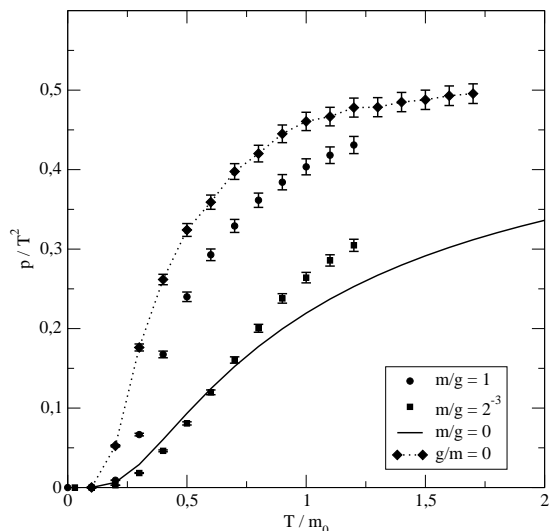


FIG. 4: Pressure as a function of temperature divided by  $T^2$  for different models: pure bose gas (solid line), stronger interacting Fermi system  $m/g = 2^{-3}$  (squares), weaker interacting Fermi system  $m/g = 1$  (circles), noninteracting Fermi gas in  $Q = 0$  sector as explained in the text (diamonds). Estimated error as explained in the text.

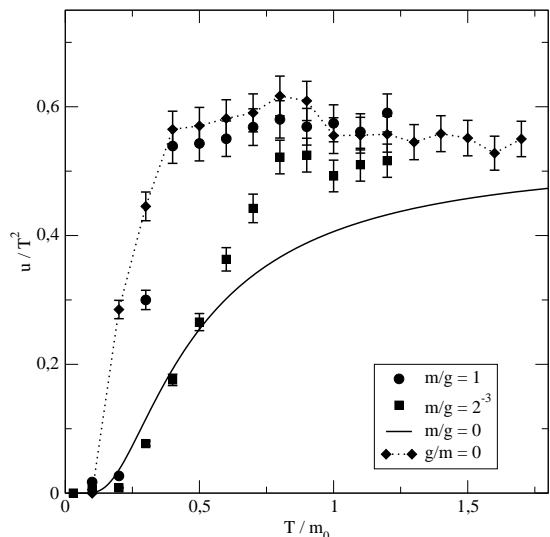


FIG. 5: Internal energy density of interacting gas as a function of temperature divided by  $T^2$ , for explanation of curves see caption of Fig. 4.

The energy density  $u$  is achieved by thermodynamic relations involving a numerical derivative of  $\ln \mathcal{Z}$ , hence error bars indicated are bigger. With the same coding  $u/T^2$  is shown in Fig. 5. In the classic ultrarelativistic limit the energy density converges to  $u/T^2 \rightarrow \pi/6$ .

The entropy density  $s = (p + u)/T$  divided by  $T$  is shown in Fig. 6 with the classical ultrarelativistic limit  $s/T \rightarrow \pi/3$ .

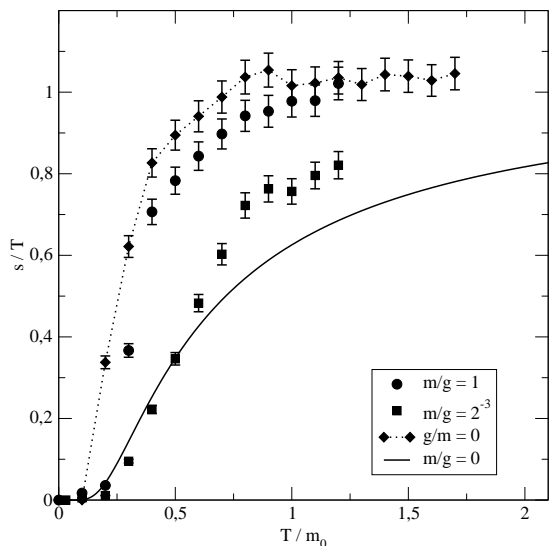


FIG. 6: Entropy density of interacting gas as a function of temperature divided by  $T$ , for explanation of curves see caption of Fig. 4.

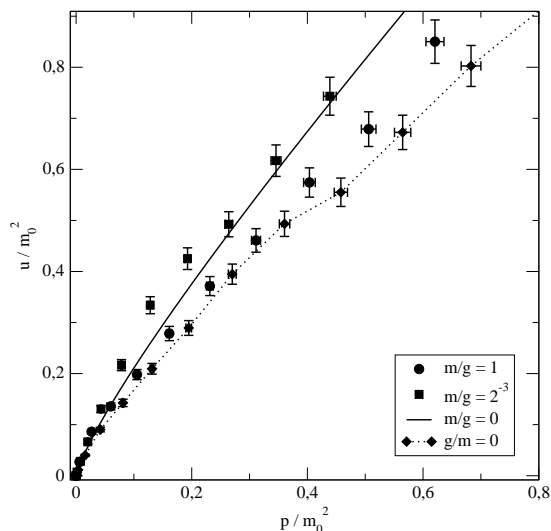


FIG. 7: Equation of state, pressure  $p$  vs. energy density  $u$  for  $\text{QED}_{1+1}$ , for explanation of curves see caption of Fig. 4. The data points belong to the following temperatures  $T/m_0 = 0.3, 0.6, 0.9, 1.2, 1.5$ .

The resulting equation of state is shown in Fig. 7. For moderate temperatures  $p \simeq 2u$ , which is taken to estimate the error in  $u$  to be twice that of  $p$ .

In conclusion, we have presented for the first time a possible way to directly evaluate the partition function of a strongly interacting relativistic system within the framework of light front quantization. To this end we have utilized DLCQ that leads to a Hamiltonian evaluated in a Fock space of finite large dimension. As an interaction we have chosen  $\text{QED}_{1+1}$ . For illustration

we have investigated some intermediate cases between the noninteracting (fermionic) limit (chemical potential  $\mu = 0$ , charge  $Q = 0$  sector) and the completely coupled (bosonic) limit of QED<sub>1+1</sub>.

Present numerical effort is manageable, i.e. all calculations have been performed on a regular PC. It is also desirable that besides evidence of feasibility further thermodynamic quantities could be calculated, such as specific heat or speed of sound. Some additional effort is needed here, since either for use of thermodynamic relations (numerical) derivatives are involved, or some quantities like energy  $U = \langle H \rangle$  have to be calculated from thermodynamic averaging. In any case within this framework it is also possible to evaluate correlation functions and deter-

mine thermal masses in a next step.

In view of demands to investigate the QCD phase transitions, the method can now be extended to QCD<sub>1+1</sub>, e.g., along the lines of [13]. A further next step along this line would be the inclusion of transverse degrees of freedom, and finally the extension to finite chemical potentials which is by construction not biased by fermion doubling and sign problems due to the generic Hamiltonian approach.

We gratefully acknowledge discussions with T. Frederico during mutual research stays at each others institutions. Work supported by the Deutsche Forschungsgemeinschaft (DFG) under contract BE1092/13.

- 
- [1] P. A. M. Dirac, *Rev. Mod. Phys.* **21**, 392 (1949).
  - [2] S. Elser and A. C. Kalloniatis, *Phys. Lett.* **B375**, 285 (1996), hep-th/9601045.
  - [3] M. Beyer, S. Mattiello, T. Frederico, and H. J. Weber, *Phys. Lett.* **B521**, 33 (2001), hep-th/0106219.
  - [4] V. S. Alves, A. Das, and S. Perez, *Phys. Rev.* **D66**, 125008 (2002), hep-th/0209036.
  - [5] H. A. Weldon, *Phys. Rev.* **D67**, 085027 (2003), hep-ph/0302147.
  - [6] A. N. Kvinikhidze and B. Blankleider, *Phys. Rev.* **D69**, 125005 (2004), hep-th/0305115.
  - [7] S. Dalley and B. van de Sande, *Phys. Rev. Lett.* **95**, 162001 (2005), hep-ph/0409114.
  - [8] J. Raufeisen and S. J. Brodsky, *Phys. Rev.* **D70**, 085017 (2004), hep-th/0408108.
  - [9] D. Rischke and G. Levin, (eds.) (2005), prepared for Workshop on New Discoveries at RHIC: The Current Case for the Strongly Interactive QGP, Brookhaven, Upton, New York, 14-15 May 2004.
  - [10] H. C. Pauli and S. J. Brodsky, *Phys. Rev.* **D32**, 1993 (1985).
  - [11] T. Eller, H. C. Pauli, and S. J. Brodsky, *Phys. Rev.* **D35**, 1493 (1987).
  - [12] C. M. Yung and C. J. Hamer, *Phys. Rev.* **D44**, 2598 (1991).
  - [13] K. Hornbostel, S. J. Brodsky, and H. C. Pauli, *Phys. Rev.* **D41**, 3814 (1990).
  - [14] Y.-z. Mo and R. J. Perry, *J. Comput. Phys.* **108**, 159 (1993).
  - [15] K. Harada, T. Heinzl, and C. Stern, *Phys. Rev.* **D57**, 2460 (1998), hep-th/9705159.
  - [16] P. Sriganesh, R. Bursill, and C. J. Hamer, *Phys. Rev.* **D62**, 034508 (2000), hep-lat/9911021.
  - [17] T. Byrnes, P. Sriganesh, R. J. Bursill, and C. J. Hamer, *Phys. Rev.* **D66**, 013002 (2002), hep-lat/0202014.
  - [18] H. Kroger and N. Scheu, *Phys. Lett.* **B429**, 58 (1998), hep-lat/9804024.
  - [19] J. R. Hiller, Y. Proestos, S. Pinsky, and N. Salwen, *Phys. Rev.* **D70**, 065012 (2004), hep-th/0407076.
  - [20] J. R. Hiller, S. Pinsky, Y. Proestos, N. Salwen, and U. Trittman (2007), hep-th/0702071.
  - [21] G. McCartor, *Z. Phys.* **C41**, 271 (1988).
  - [22] F. Lenz, M. Thies, K. Yazaki, and S. Levit, *Annals Phys.* **208**, 1 (1991).
  - [23] L. Martinovic, *Phys. Lett.* **B400**, 335 (1997).
  - [24] P. C. Hohenberg, *Phys. Rev.* **158** (1967).